Control of a Mechanically Compliant Joint with Proportional-Integral-Retarded (PIR) Controller

Xixian Mo, Feng Jiang, Wenhui Wang, Bo Zhang(✉), and Ye Ding

State Key Laboratory of Mechanical System and Vibration,
School of Mechanical Engineering, Shanghai Jiao Tong University,
Shanghai 200240, China
{wanjushengfang,f.jiang,15026686939,b_zhang,y.ding}@sjtu.edu.cn

Abstract. In this paper, a mechanically compliant joint is designed and a novel proportional-integral-retarded (PIR) controller is adopted. Firstly, the structure of the invariant stiffness joint is introduced in details and linear springs are connected with the output link to obtain flexibility. Secondly, the control programs are built with Simulink and automatically compiled and downloaded into the controller. Thirdly, the physical mechanism and electromagnetic function of permanent magnet synchronous motor (PMSM) are combined to get the transfer function. Fourthly, a direct integration method (DIM) with Simpson method is proposed and used to analyze the stability of PIR controller with the joint. Finally, some compared experiments with conventional proportional-integral-derivative (PID) controller added a low-pass filter in the derivative term in speed loop and position loop are taken, and the results show that PIR controller is better in the speed of settlement and more stable in some condition.

Keywords: Mechanically compliant joint · PIR · DIM

1 Introduction

Robot compliance characteristic plays an important role in the interaction between robots and human or environment to ensure the safety of operation. The compliance or stiffness of robot joints can be obtained from the force control of rigid joints with torque sensors or compliant joints based on mechanical system like springs [5]. Because of the good performance of the bandwidth of force input and energy efficiency [4,13], the mechanically compliant joints have been widely studied in recent decades. Humanoid robots with mechanically compliant systems may have wide applications in fields like service, education and health care.

One type of mechanically compliant joints have invariant stiffness like Domo [2] and the Robonaut 2 (R2) designed by the National Aeronautics and Space

Z. Chen et al. (Eds.): ICIRA 2018, LNAI 10984, pp. 379–390, 2018.
https://doi.org/10.1007/978-3-319-97586-3_34

Administration (NASA) [1]. Another type of joints have variable stiffness like the Floating Spring Joint (FSJ) from Deutsches Zentrum für Luft- und Raumfahrt (DLR) (German Aerospace Center in English) [12], hybrid dual actuator unit (HDAU) [5] and The CompAct-VSA unit designed by Istituto Italiano di Tecnologia (IIT) (Italian Institute of Technology in English) [9]. There is only one motor in invariant stiffness joints to keep the output position that results in advantages in cost, weight and size while the stiffness cannot be adapted [8]. Variant stiffness joints have one motor to keep the position of the output and another motor to adjust the stiffness of the joint, so they can be used in different tasks because of the adaptable stiffness [6]. Considering the invariant stiffness joints are lighter, smaller and cost less, an invariant stiffness joint using linear springs with constant elastic coefficient as elastic elements was designed.

Recently, a novel type of controller called proportional-integral-retarded (PIR) controller is proposed [7,10]. For n-th order linear time-invariant (LTI) system with PIR controller

$$\begin{cases} x^{(n)}(t) + \sum\limits_{k=0}^{n-1} a_k x^{(k)}(t) = \sum\limits_{k=0}^{n-1} b_k u^{(k)}(t) \\ u(t) = k_p e(t) + k_i \int_0^t e(\tau) d\tau - k_r e(t - t_r) \end{cases} \tag{1}$$

where $u(t)$ is the input, $x(t)$ is the output, $e(t) = r(t) - x(t)$ is the error, $r(t)$ is the reference and $e(t < 0) = 0$. k_p is the proportional gain, k_i is the integral gain, k_r is the retarded gain, and $t_r > 0$ is the delayed error. The difference between PIR controller and conventional PID controller is that the derivative term is replaced by a former error, thus noise amplification by derivation is avoided. In order to analyze the stability of PIR controller, direct integration method (DIM) is used [11]. Typically, time delay is approximated by Pade approximation to a rational function but losing accuracy when the delay is long and needs high order approximation. Frequency domain study on second order LTI systems has been taken [7], but not appropriate for higher order systems.

The rest of this paper is organized as follows. The design and model of the mechanically compliant joint are in Sect. 2. In Sect. 3, stability analysis with DIM on PIR controller is presented. Some experiments are taken and results are analyzed in Sect. 4, followed by the conclusion in Sect. 5.

2 Mechanically Compliant Joint

Figures 1 and 2 shows the structure of the joint. The joint consists a motor, a harmonic drive and a passive compliant module. The passive compliant module is fixedly connected with the output of the harmonic drive. An output link is connect to the base of the module with four linear springs. Given the physical mechanisms of the mechanically compliant joint, a linear torsion spring model approximately describes the flexibility of the joint. When the rotation angle of the output link is different with the output of harmonic drive, the passive

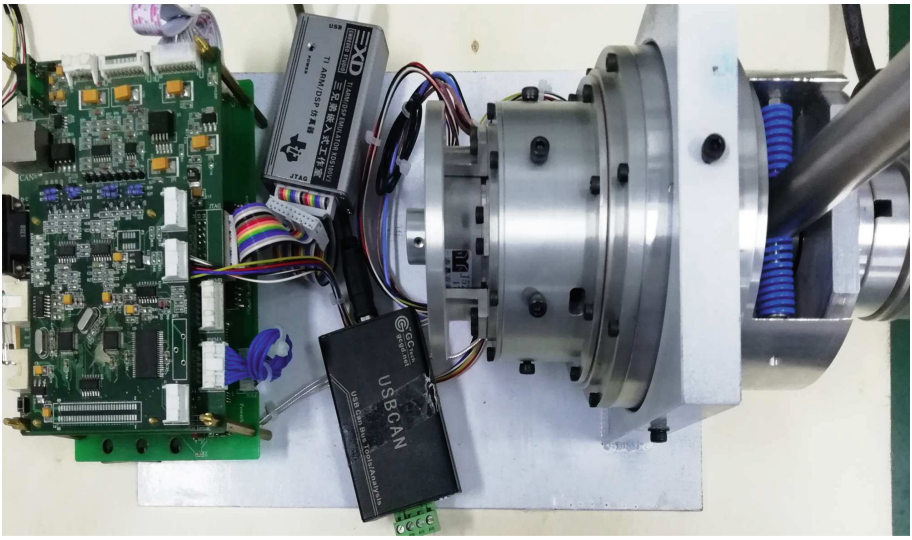

Fig. 1. Mechanically compliant joint.

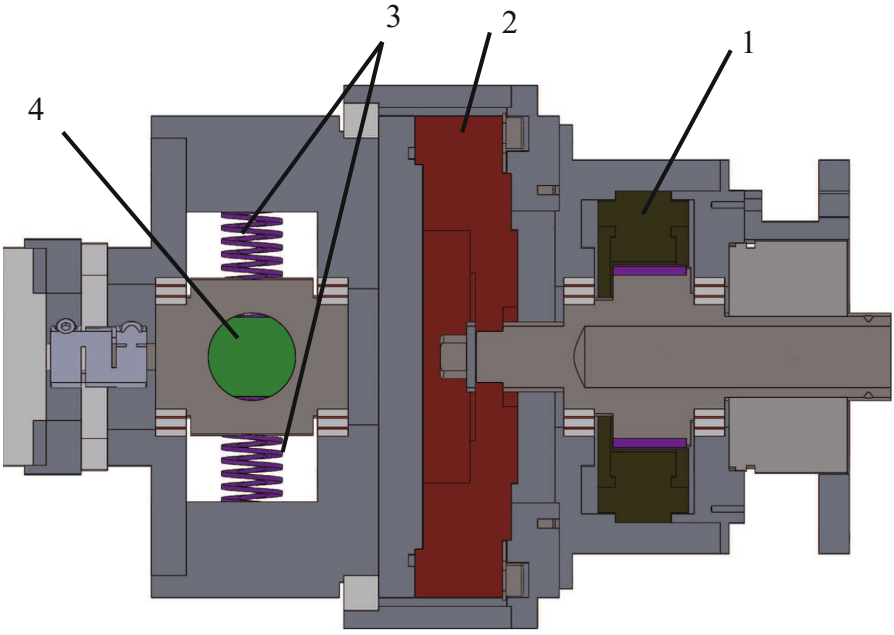

1. PMSM; 2. Harmonic drive; 3. Linear springs; 4. Extended output link.

Fig. 2. Section view of the joint.

compliant module products a torque which has linear relationship with the rotation angle difference, and the spring torque is

$$\tau_k = k(\frac{\theta_m}{r} - \theta_l) \tag{2}$$

where k is the spring's torsion coefficient, θ is the rotation angle when subscript m represents motor and subscript l represents the link, and r is the gearing reduction ratio.

At the motor side and the link side, assume there is no load and perform the torque balance

$$j_m\ddot{\theta}_m + b_m\dot{\theta}_m = \tau_m - \tau_k \tag{3}$$

$$j_l\ddot{\theta}_l + b_l\dot{\theta}_l = \tau_k \tag{4}$$

where j is the moment of inertia, b is the damping coefficient, and τ_m is the motor torque.

The model of the PMSM is described in direct (d) and quadrature (q) rotating coordinate system by

$$u_d = L_d\dot{i_d} + Ri_d - p\dot{\theta}_m L_q i_q \tag{5}$$

$$u_q = L_q\dot{i_q} + Ri_q + p\dot{\theta}_m(L_d i_d + \psi) \tag{6}$$

$$\tau_m = \frac{3}{2}pi_q((L_d - L_q)i_d + \psi) \tag{7}$$

where u_d and u_q are d axis and q axis voltage components, i_d and i_q are d axis and q axis current components, L_d and L_q are d axis and q axis inductance components, R is the stator resistance, p is the motor pole pairs, and ψ is the permanent magnet flux linkage.

In order to simplify the system, PI controllers are used in current loops for controlling i_d to zero, and u_q is approximately proportional to i_q, so

$$u_q = k_q i_q \tag{8}$$

$$\tau_m = k_u u_q \tag{9}$$

After Laplace transformation, transfer function between input u_q and output θ_l is

$$P(s) = \frac{\Theta_l(s)}{U_q(s)} = \frac{k_u k}{(rj_m s^2 + rb_m s + k)(j_l s^2 + b_l s + k) - k^2} \tag{10}$$

Notice that the model is a fourth order system with four poles and no zeros. For a large number of experiments and comparisons, the best identification can be given as follows:

$$\frac{7.148 \times 10^6}{s^4 + 130.2s^3 + 2.671 \times 10^4 s^2 + 6.030 \times 10^5 s + 4261} \tag{11}$$

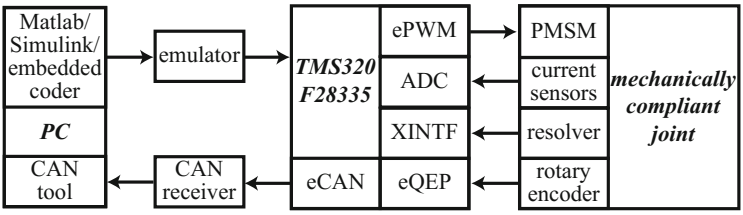

Fig. 3. Scheme of control and sensor system.

Figure 3 shows the control and sensor system. The main chip is a microcontroller TMS320F28335 from Texas Instruments. In general, programs are developed with C program language and debugged in the integrated development environment (IDE) named Code Composer Studio (CCS), but a more convenient way is developing with block diagram in the Matlab/Simulink environment and building by embedded coder toolbox. Applications are automatically compiled, downloaded through emulator and executed by only one click.

There are many integrated peripherals in F28335. With space vector pulse-width modulation (SVPWM), desired d axis and q axis voltage are encoded into pulse signals by enhanced pulse-width modulation (ePWM) modules to control six metal-oxide-semiconductor field-effect transistors (MOSFET). When the PMSM is actuated, the harmonic drive reduces speed and the output link of the joint waves. There are three types of sensors for data acquisition. Firstly, currents are detected by two current sensors Honeywell CSNE151-100 based on Hall effect and converted into digital signals by the analog-to-digital converter (ADC) module. Secondly, the position of motor from a resolver on the PMSM is read through external interface (XINTF). Finally, a rotary encoder ROD 486 from HEIDENHAIN gets the rotation angle of the output link and transferred to enhanced quadrature encoder (eQEP) module. When the program is running, the enhanced controller area network (eCAN) module sends data in 1 Mbps to PC through a CAN receiver and a CAN tool software.

3 DIM on PIR Controller

In the system Eq. 1 with PIR controller, assume $r(t) = 0$, then

$$x^{(n+1)}(t) + \sum_{i=0}^{n} c_i x^{(i)}(t) - \sum_{j=1}^{n} k_r b_{j-1} x^{(j)}(t - t_r) = 0 \tag{12}$$

where $c_0 = k_i b_0$, $c_n = a_{n-1} + k_p b_{n-1}$, $c_k = a_{k-1} + k_p b_{k-1} + k_i b_k (k = 1, ..., n-1)$.

Let $\boldsymbol{X}(t) = [x(t), \dot{x}(t), ..., x^{(n)}(t)]^T$, then

$$\dot{\boldsymbol{X}}(t) = \boldsymbol{B}\boldsymbol{X}(t - t_r) + \boldsymbol{C}\boldsymbol{X}(t) \tag{13}$$

where

$$\boldsymbol{B} = k_r \begin{pmatrix} & \mathbf{0}_{n\times(n+1)} & \\ 0\ b_0 & \cdots & b_{n-1} \end{pmatrix}, \boldsymbol{C} = \begin{pmatrix} 0 & 1 & & \\ & & \ddots & \\ & & & 1 \\ -c_0 & -c_1 & \ldots & -c_n \end{pmatrix} \tag{14}$$

Assume the sample time is $\delta < t_r$ and the time period $[t - t_r, t]$ is separated into $t_k = t - t_r + \frac{k}{2}\delta (k = 0, 1, ..., N)$ ($N = \langle 2t_r/\delta \rangle$, $\langle x \rangle$ means the nearest even integer of x). So

$$\dot{\boldsymbol{X}}(t) = \boldsymbol{B}\boldsymbol{X}(t - t_r) + \boldsymbol{C}(\boldsymbol{X}(t_k) + \int_{t_k}^{t} \dot{\boldsymbol{X}}(\tau)d\tau) \tag{15}$$

If numerically integrated by the trapezoidal rule at the start and the Simpson's rule with the rest, then

$$\begin{cases} \dot{\boldsymbol{X}}(t_0) = \boldsymbol{B}\boldsymbol{X}(t_0 - t_r) + \boldsymbol{C}\boldsymbol{X}(t_0) \\ \dot{\boldsymbol{X}}(t_1) = \boldsymbol{B}\boldsymbol{X}(t_1 - t_r) + \boldsymbol{C}\boldsymbol{X}(t_0) + \frac{\delta}{2}\boldsymbol{C}(\dot{\boldsymbol{X}}(t_0) + \dot{\boldsymbol{X}}(t_1)) \\ \dot{\boldsymbol{X}}(t_i) = \boldsymbol{B}\boldsymbol{X}(t_i - t_r) + \boldsymbol{C}\boldsymbol{X}(t_{i-2}) + \frac{\delta}{6}\boldsymbol{C}(\dot{\boldsymbol{X}}(t_{i-2}) + 4\dot{\boldsymbol{X}}(t_{i-1}) + \dot{\boldsymbol{X}}(t_i)) \\ (i = 2, ..., N) \end{cases} \tag{16}$$

Let $\mathcal{Z}(t) = [\boldsymbol{X}(t_0)^T, \boldsymbol{X}(t_1)^T, ..., \boldsymbol{X}(t_N)^T]^T$, so

$$\boldsymbol{D}\dot{\mathcal{Z}}(t) = \boldsymbol{E}\mathcal{Z}(t - t_r) + \boldsymbol{F}\mathcal{Z}(t) \tag{17}$$

where

$$\boldsymbol{D} = \begin{pmatrix} \boldsymbol{I}_{n+1} & & & & \\ -\frac{\delta}{2}\boldsymbol{C} & \boldsymbol{I}_{n+1} - \frac{\delta}{2}\boldsymbol{C} & & & \\ -\frac{\delta}{6}\boldsymbol{C} & -\frac{4\delta}{6}\boldsymbol{C} & \boldsymbol{I}_{n+1} - \frac{\delta}{6}\boldsymbol{C} & & \\ & \ddots & \ddots & \ddots & \\ & & -\frac{\delta}{6}\boldsymbol{C} & -\frac{4\delta}{6}\boldsymbol{C} & \boldsymbol{I}_{n+1} - \frac{\delta}{6}\boldsymbol{C} \end{pmatrix} \tag{18}$$

$$\boldsymbol{E} = \begin{pmatrix} \boldsymbol{B} & & \\ & \ddots & \\ & & \boldsymbol{B} \end{pmatrix} \tag{19}$$

$$\boldsymbol{F} = \begin{pmatrix} \boldsymbol{C} & & & \\ \boldsymbol{C} & & & \\ \boldsymbol{C} & & & \\ & \ddots & & \\ & & \boldsymbol{C}\ \mathbf{0}_{n+1} & \mathbf{0}_{n+1} \end{pmatrix} \tag{20}$$

$\boldsymbol{I}_{n+1}$ is the identity matrix of size $n + 1$.

In the period $[t_0, t]$,

$$\boldsymbol{X}(t) = \boldsymbol{X}(t_k) + \int_{t_k}^{t} \dot{\boldsymbol{X}}(\tau) d\tau \tag{21}$$

also using the numerical integration,

$$\begin{cases} \boldsymbol{X}(t_1) = \boldsymbol{X}(t_0) + \frac{\delta}{2}(\dot{\boldsymbol{X}}(t_0) + \dot{\boldsymbol{X}}(t_1)) \\ \dot{\boldsymbol{X}}(t_i) = \boldsymbol{X}(t_{i-2}) + \frac{\delta}{6}\boldsymbol{C}(\dot{\boldsymbol{X}}(t_{i-2}) + 4\dot{\boldsymbol{X}}(t_{i-1}) + \dot{\boldsymbol{X}}(t_i))(i = 2, ..., N) \end{cases} \tag{22}$$

So

$$\boldsymbol{G}\dot{\mathbb{Z}}(t) = \boldsymbol{H}\mathbb{Z}(t) \tag{23}$$

where

$$\boldsymbol{G} = \begin{pmatrix} \boldsymbol{0}_{n+1} & & & \\ \frac{\delta}{2}\boldsymbol{I}_{n+1} & \frac{\delta}{2}\boldsymbol{I}_{n+1} & & \\ \frac{\delta}{6}\boldsymbol{I}_{n+1} & \frac{4\delta}{6}\boldsymbol{I}_{n+1} & \frac{\delta}{6}\boldsymbol{I}_{n+1} & \\ & \ddots & \ddots & \ddots \\ & & \frac{\delta}{6}\boldsymbol{I}_{n+1} & \frac{4\delta}{6}\boldsymbol{I}_{n+1} \quad \frac{\delta}{6}\boldsymbol{I}_{n+1} \end{pmatrix} \tag{24}$$

$$\boldsymbol{H} = \begin{pmatrix} \boldsymbol{0}_{n+1} & & & \\ -\boldsymbol{I}_{n+1} & \boldsymbol{I}_{n+1} & & \\ -\boldsymbol{I}_{n+1} & \boldsymbol{0}_{n+1} & \boldsymbol{I}_{n+1} & \\ & \ddots & \ddots & \ddots \\ & & -\boldsymbol{I}_{n+1} & \boldsymbol{0}_{n+1} \quad \boldsymbol{I}_{n+1} \end{pmatrix} \tag{25}$$

With Eqs. 17 and 23,

$$(\boldsymbol{H} - \boldsymbol{G}\boldsymbol{D}^{-1}\boldsymbol{F})\mathbb{Z}(t) = (\boldsymbol{G}\boldsymbol{D}^{-1}\boldsymbol{E})\mathbb{Z}(t - t_r) \tag{26}$$

Equation 26 cannot be solved because it is an indeterminate equation, thus adding the continuity (i.e. $\boldsymbol{X}(t_0) = \boldsymbol{X}(t_N - t_r)$)

$$\boldsymbol{P}\mathbb{Z}(t) = \boldsymbol{Q}\mathbb{Z}(t - t_r) \tag{27}$$

where

$$\boldsymbol{P} = \begin{pmatrix} \boldsymbol{I}_{n+1} \\ \boldsymbol{0} \end{pmatrix}, \boldsymbol{Q} = \begin{pmatrix} \boldsymbol{I}_{n+1} \\ \boldsymbol{0} \end{pmatrix} \tag{28}$$

then

$$\mathbb{Z}(t) = \boldsymbol{\Phi}\mathbb{Z}(t - t_r) \tag{29}$$

where

$$\boldsymbol{\Phi} = (\boldsymbol{H} - \boldsymbol{G}\boldsymbol{D}^{-1}\boldsymbol{F} + \boldsymbol{P})^{-1}(\boldsymbol{G}\boldsymbol{D}^{-1}\boldsymbol{E} + \boldsymbol{Q}) \tag{30}$$

$\boldsymbol{\Phi}$ is the transition matrix. According to Floquet theory, the system is stable when all modules of eigenvalues of $\boldsymbol{\Phi}$ is less than one [3]. In other words, if λ presents eigenvalue function, then

$$\max(|\lambda(\boldsymbol{\Phi})|) < 1 \tag{31}$$

In order to demonstrate DIM is as reliable as frequency domain method, an analyzed system by Ramírez et al. [7] is taken as an example (Fig. 4).

Example. $n = 2$, $a_1 = 0.45056$, $a_0 = 309.76$, $b_1 = 0$, $b_0 = 31$, $k_p = 22.57$, $k_i = 0$, find stable region in the (t_r, k_r) space.

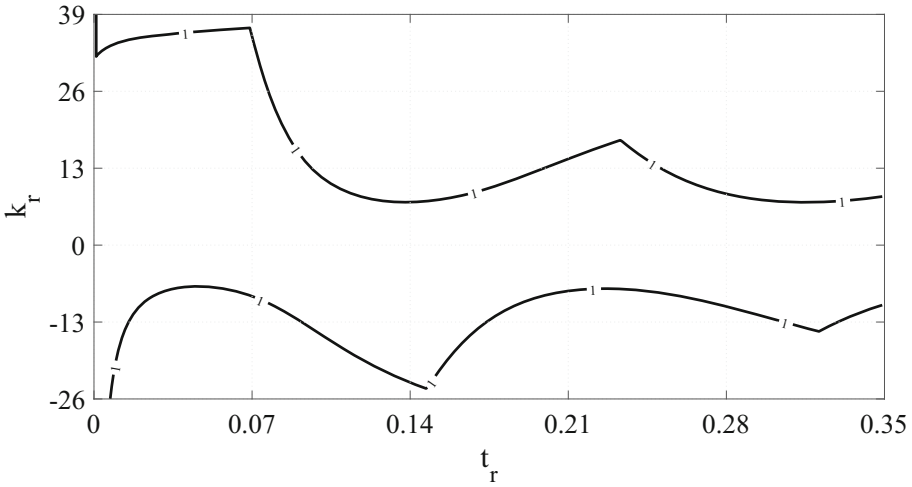

Fig. 4. Stable region of example.

4 Experiment

Figure 5 shows the block diagram of experiments. In order to control the position of the link, two controllers based on errors are used in position loop $F(s)$ and speed loop $H(s)$ and two types of controllers are compared: PIR and PIDN. PIDN controller is a conventional PID controller added a low-pass filter with coefficient N in the derivative term to filter noise and sudden reference signal change, and the transfer function is

$$k_p + \frac{k_i}{s} + k_d s \frac{N}{s+N} \tag{32}$$

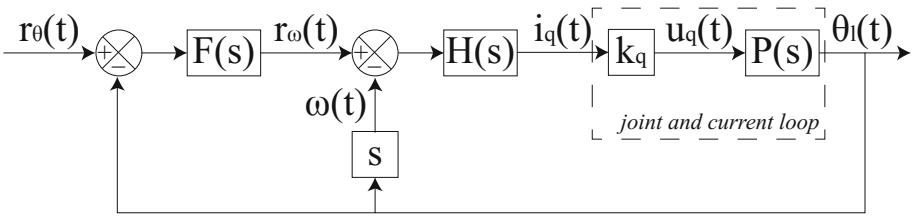

Fig. 5. Block diagram of experiments.

There are four parameters in both controllers, and parameters tuning is performed through minimizing the integral time absolute error (ITAE) function

$$ITAE = \int_0^T t|e(t)|dt \tag{33}$$

Because the ITAE function is hard to calculate derivative, a derivative-free Nelder-Mead method is used. In order to protect the joint, stability is analyzed by DIM before taking experiment.

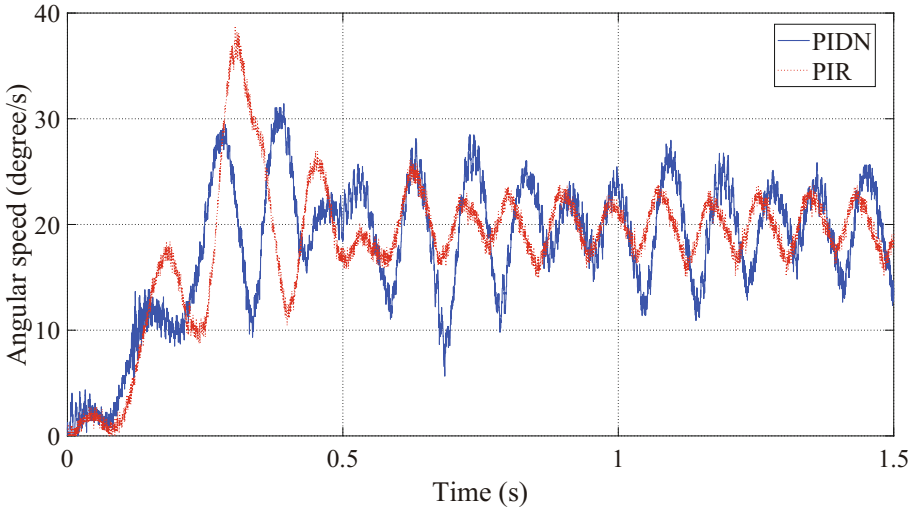

Fig. 6. Experiment results in speed loop.

Table 1. Experiment results in speed loop.

Speed loop controller	ITAE (T = 4s)
PIDN	14.32
PIR	9.51

Figure 6 and Table 1 show the optimal results in speed loop. Due to the amplification of noise and disturbance when using position difference to obtain speed, both angular speeds are oscillating around given speed 20 degree/s, but obviously the amplitude of oscillation and ITAE of PIR controller are smaller than those of PIDN controller.

The optimal results in position loop are shown in Fig. 7 and Table 2 when the parameters of controllers in speed loop are not tuned again. The results prove that using PIR controller in speed loop is much better than PIDN controller no

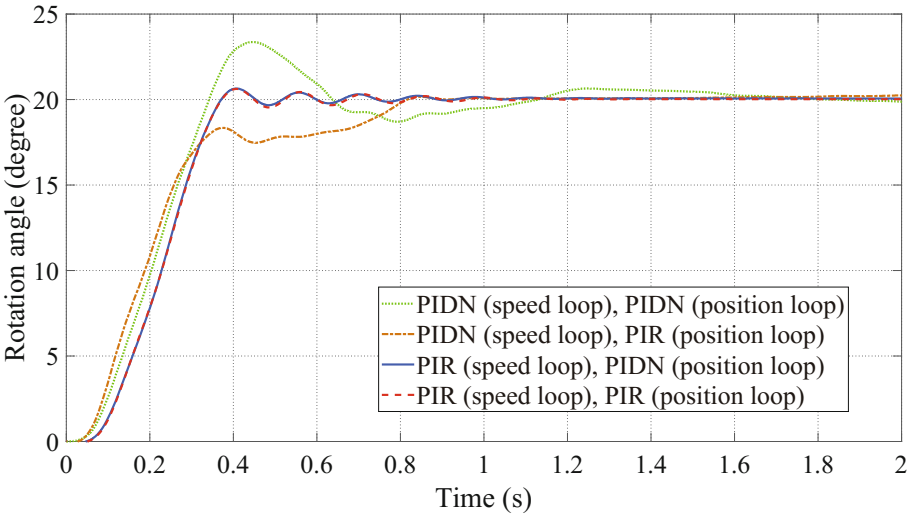

Fig. 7. Experiment results in position loop.

Table 2. Experiment results in position loop.

Speed loop controller	Position loop controller	ITAE (T = 4s)	2% settling time (s)
PIDN	PIDN	1.518	1.548
PIDN	PIR	2.001	0.788
PIR	PIDN	1.028	0.563
PIR	PIR	0.799	0.571

matter which controller is used in position loop. When using PIR controller in speed loop, the performance of PIR controller and PIDN controller in position loop is almost the same. Even though using PIDN controller in speed loop, ITAE and settling time of PIR controller in position loop is smaller than those of PIDN controller. The conclusion is PIR controller is better in the speed of settlement and more stable than PIDN controller in some condition.

5 Conclusion

This paper presents a mechanically compliant joint. The joint is designed with linear springs to obtain flexibility. Physical model and the characteristic of PMSM are combined to get the transfer function. A PIR controller is proposed and DIM is used to analyze the stability. The compared experiment results show that PIR controller is better in the speed of settlement and more stable than PIDN controller in some condition. In the speed loop, the amplitude of oscillation and ITAE of PIR controller are smaller than those of PIDN controller. When

using PIDN controller in speed loop, ITAE and settling time of PIR controller in position loop is smaller than those of PIDN controller. In the future work, some global optimization like generic algorithm and particle swarm optimization may be used to optimize the parameters of controllers in speed loop and position loop at the same time.

Acknowledgments. This work was supported by the National Natural Science Foundation of China under grant 91648112 for which the authors are grateful.

References

1. Diftler, M.A., et al.: Robonaut 2 - the first humanoid robot in space. In: 2011 IEEE International Conference on Robotics and Automation, pp. 2178–2183, May 2011. https://doi.org/10.1109/ICRA.2011.5979830
2. Edsinger, A.: Robot manipulation in human environments (2007)
3. Farkas, M.: Periodic Motions, vol. 104. Springer, New York (2013)
4. Hurst, J.W., Chestnutt, J.E., Rizzi, A.A.: An actuator with physically variable stiffness for highly dynamic legged locomotion. In: Proceedings of the IEEE International Conference on Robotics and Automation, ICRA 2004, vol. 5, pp. 4662–4667, April 2004. https://doi.org/10.1109/ROBOT.2004.1302453
5. Kim, B.S., Song, J.B.: Hybrid dual actuator unit: a design of a variable stiffness actuator based on an adjustable moment arm mechanism. In: 2010 IEEE International Conference on Robotics and Automation, pp. 1655–1660, May 2010. https://doi.org/10.1109/ROBOT.2010.5509264
6. Park, J.J., Kim, H.S., Song, J.B.: Safe robot arm with safe joint mechanism using nonlinear spring system for collision safety. In: 2009 IEEE International Conference on Robotics and Automation, pp. 3371–3376, May 2009. https://doi.org/10.1109/ROBOT.2009.5152268
7. Ramrez, A., Mondi, S., Garrido, R., Sipahi, R.: Design of proportional-integral-retarded (PIR) controllers for second-order LTI systems. IEEE Trans. Autom. Control **61**(6), 1688–1693 (2016). https://doi.org/10.1109/TAC.2015.2478130
8. Tsagarakis, N.G., Laffranchi, M., Vanderborght, B., Caldwell, D.G.: A compact soft actuator unit for small scale human friendly robots. In: 2009 IEEE International Conference on Robotics and Automation, pp. 4356–4362, May 2009. https://doi.org/10.1109/ROBOT.2009.5152496
9. Tsagarakis, N.G., Sardellitti, I., Caldwell, D.G.: A new variable stiffness actuator (compact-VSA): Design and modelling. In: 2011 IEEE/RSJ International Conference on Intelligent Robots and Systems, pp. 378–383, September 2011. https://doi.org/10.1109/IROS.2011.6095006
10. Villafuerte, R., Mondi, S., Garrido, R.: Tuning of proportional retarded controllers: theory and experiments. IEEE Trans. Control Syst. Technol. **21**(3), 983–990 (2013). https://doi.org/10.1109/TCST.2012.2195664
11. Wen, Z., Ding, Y., Liu, P., Ding, H.: Direct integration method for time-delayed control of second-order dynamic systems. J. Dyn. Syst. Measur. Control **139**(6), 061001 (2017). https://doi.org/10.1115/1.4035359

12. Wolf, S., Eiberger, O., Hirzinger, G.: The DLR FSJ: Energy based design of a variable stiffness joint. In: 2011 IEEE International Conference on Robotics and Automation, pp. 5082–5089, May 2011. https://doi.org/10.1109/ICRA.2011.5980303
13. Zinn, M., Khatib, O., Roth, B., Salisbury, J.K.: Playing it safe [human-friendly robots]. IEEE Robot. Autom. Mag. **11**(2), 12–21 (2004). https://doi.org/10.1109/MRA.2004.1310938